

## Improvement on output torque of dielectric elastomer minimum energy structures

Jianwen Zhao, Junyang Niu, David McCoul, Yong Ge, Qibing Pei, Liwu Liu, and Jinsong Leng

Citation: *Appl. Phys. Lett.* **107**, 063505 (2015);

View online: <https://doi.org/10.1063/1.4928629>

View Table of Contents: <http://aip.scitation.org/toc/apl/107/6>

Published by the [American Institute of Physics](#)

---

### Articles you may be interested in

[Phenomena of nonlinear oscillation and special resonance of a dielectric elastomer minimum energy structure rotary joint](#)

*Applied Physics Letters* **106**, 133504 (2015); 10.1063/1.4915108

[Multi-functional dielectric elastomer artificial muscles for soft and smart machines](#)

*Journal of Applied Physics* **112**, 041101 (2012); 10.1063/1.4740023

[A review on dielectric elastomer actuators, technology, applications, and challenges](#)

*Journal of Applied Physics* **104**, 071101 (2008); 10.1063/1.2981642

[Modeling a dielectric elastomer as driven by triboelectric nanogenerator](#)

*Applied Physics Letters* **110**, 033505 (2017); 10.1063/1.4974143

[Energy minimization for self-organized structure formation and actuation](#)

*Applied Physics Letters* **90**, 081916 (2007); 10.1063/1.2695785

[Method to analyze electromechanical stability of dielectric elastomers](#)

*Applied Physics Letters* **91**, 061921 (2007); 10.1063/1.2768641

---

**Scilight**

Sharp, quick summaries **illuminating**  
the latest physics research

Sign up for **FREE!**



## Improvement on output torque of dielectric elastomer minimum energy structures

Jianwen Zhao,<sup>1,2,3,a)</sup> Junyang Niu,<sup>2</sup> David McCoul,<sup>3</sup> Yong Ge,<sup>2</sup> Qibing Pei,<sup>3</sup> Liwu Liu,<sup>1</sup> and Jinsong Leng<sup>1</sup>

<sup>1</sup>Postdoctoral Research Station of Material Science and Engineering, Harbin Institute of Technology, Harbin 157401, China

<sup>2</sup>Department of Mechanical Engineering, Harbin Institute of Technology, Weihai 264209, China

<sup>3</sup>Department of Materials Science and Engineering, UCLA, Los Angeles, California 90095, USA

(Received 1 June 2015; accepted 3 August 2015; published online 14 August 2015)

The dielectric elastomer minimum energy structure (DEMES) can realize large angular deformations by a small voltage-induced strain of the dielectric elastomer (DE), so it is a suitable candidate to make a rotary joint for a soft robot. However, the payload capacity of a DEMES joint is small compared with other types of dielectric elastomer actuators. Stacking layers of pre-strained DE thin films can increase the output torque of DEMES, but greater driving power will be needed, limiting application in mobile or flying soft robots. In this paper, based on static analysis, a design of DEMES is proposed that has larger torque than the traditional design with the same number of layers of dielectric elastomer. As an experimental example, the torque of the film with the improved design is larger than 1.7 times that of the traditional design. Experiments validate the theoretical analysis and demonstrate the improvement of DEMES output torque. © 2015 AIP Publishing LLC. [<http://dx.doi.org/10.1063/1.4928629>]

As a novel kind of actuator, the dielectric elastomer (DE) demonstrates high-strain response,<sup>1</sup> high energy densities (seventy times higher than conventional electromagnetic actuators),<sup>2</sup> and high energy conversion efficiencies (the peak theoretical value is 60%–90% (Ref. 3)). The dielectric elastomer minimum energy structure (DEMES) is a kind of DE actuator proposed by Kofod *et al.*<sup>4</sup> and has attracted much attention.<sup>5,6</sup> The simplified mechanism of DEMES is shown in Figure 1. After adhering a pre-stretched DE film to a thin elastic frame such as polyethylene terephthalate (PET),<sup>7</sup> acrylonitrile butadiene styrene (ABS),<sup>8</sup> or polyvinyl chloride (PVC),<sup>9</sup> the restoring force of the film bends the elastic frame into a minimum energy state. When kilovolts of low-current electricity are applied across the dielectric elastomer, the frame flattens out and the bending angle decreases. In this way, dynamically changing the voltage can dynamically and continuously alter the joint angle. This shows much potential for flapping wings,<sup>10</sup> soft robotic systems,<sup>11,12</sup> and deployable microsatellite grippers.<sup>13</sup>

There is also a restriction on output torque that limits the application of DEMES. Compared with other DE actuators, the payload capacity of a DEMES joint is small with a single layer of DE film. If we stack layers of films to increase the output torque of DEMES joint, the total capacitance of the actuator will increase and will require greater power supply, limiting its application in mobile or flying robots. For a DE flapping wing, experiments indicate that the response of three layers of VHB<sup>TM</sup> 4910 is slower than that of two layers (using an applied square wave voltage with 3–5 kV amplitude and the duty cycle of 0.5). Therefore, we should explore a design to increase the output torque of DEMES with limited layers of DE films. To explore this design, static analysis

should be carried out to investigate the characteristics of the output torque.

A reference coordinate system is shown in Figure 2. The origin  $O$  is placed at the centroid of the elliptical hollow area. The  $z$ -axis is perpendicular to the plane of the frame.

As shown in Figure 2 (right), the edge of the film is in a state of tensile stress  $F$  that creates a force component in the  $z$ -direction. Consequently, the film warps like a saddle under the force component  $F_z$ . The natural morphology of the DE film at the central elliptical hole of the frame is depicted in Figure 3.

It can be speculated from the saddle surface morphology that the gradient of this saddle surface at points  $M_{1-4}$  on boundary  $ABCD$  is zero. The tension force on boundary  $M_1AM_4$  can be simplified to an equivalent composite force at point  $A$  called  $F_r$ . Similarly, the tension force on boundaries  $M_1BM_2$ ,  $M_2CM_3$ , and  $M_3DM_4$  can be simplified to equivalent forces acting at points  $B$ ,  $C$ , and  $D$ . By symmetry, the tension force at point  $A$  equals that at point  $C$ , and the force at  $B$  equals that at  $D$ . Force  $F_r$  has a positive component along the  $z$ -axis in the  $xz$ -plane. Force  $F_R$  has a negative component along the  $z$ -axis in the  $yz$ -plane. The magnitude of the component of  $F_r$  in the positive  $z$ -direction  $F_{r-z}$  is greater than the magnitude of the component of  $F_R$  in the negative  $z$ -direction  $F_{R-z}$  before the film buckled, because  $F_{R-z} = 0$ . The result causes the DE film to buckle upwards.  $F_{r-z}$  is decreasing while  $F_{R-z}$  is increasing with buckling upwards. The height of the film buckle is determined when  $F_{r-z}$  and  $F_{R-z}$  reach static equilibrium. The DE saddle on a DEMES is shown in Figure 4.

To restrict frame bending to only one axis, the rigidity of the non-bending edges was enhanced by mounting two stiffening beams as shown in Ref. 14 and Figure 5, because the DE film is biaxially prestretched to ensure sufficient

<sup>a)</sup>Email: zhaojianwen@hit.edu.cn

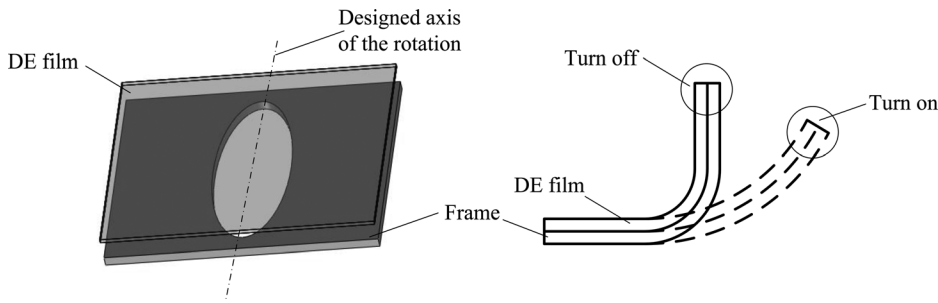


FIG. 1. Deformation principle of the DEMES rotary joint.

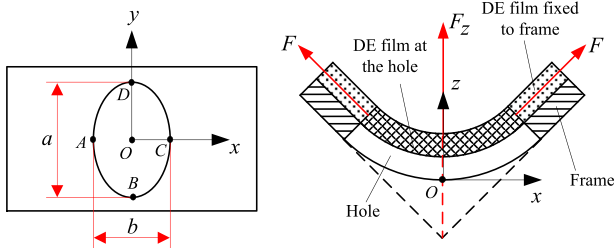


FIG. 2. Top view (left) and cross section (right) of the structure.

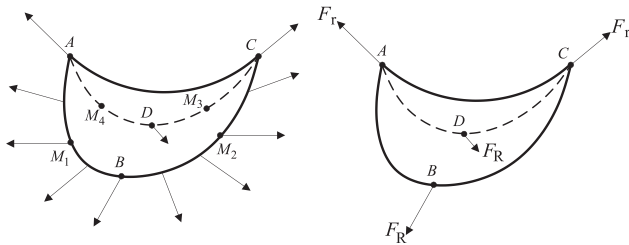


FIG. 3. Free body diagrams of the active DE saddle. (a) Representative forces at the edges of the DE film saddle. (b) Equivalent forces at select points.

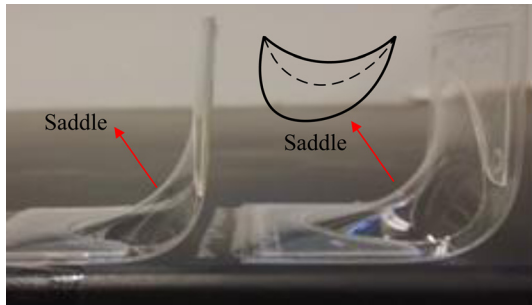


FIG. 4. Picture of DE saddle on a DEMES.

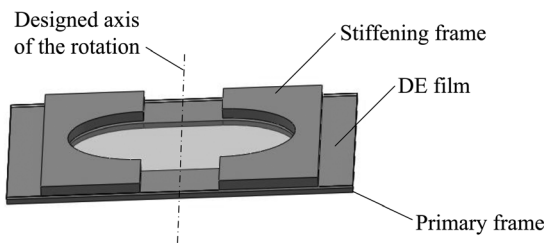


FIG. 5. The DEMES rotary joint with semicircular stiffening elements.

voltage-induced strain and to avoid snap-through electromechanical instability.

We define the parameters of the structure (see Fig. 5) in Figure 6.

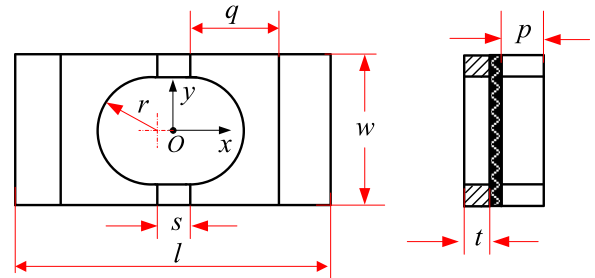


FIG. 6. Parameters of the structure.  $l$  = total length,  $w$  = total width,  $t$  = thickness of primary frame (exaggerated),  $p$  = thickness of stiffening frame (exaggerated),  $q$  = width of each stiffening frame,  $s$  = spacing between the stiffening frame, and  $r$  = radius of each semicircle.

In Figure 6, the thicknesses of the primary frame, film, and stiffening frame are greatly exaggerated to show the structure more clearly.

The initial thickness of the DE film (VHB 4910) is 1 mm, and after 400% biaxial prestrain the thickness has changed to 40–50  $\mu\text{m}$  due to the incompressibility of the elastomer. Because the dimension of parameters  $a$  and  $b$  is at least 10 mm in the general application, the thickness of the DE can be neglected when the static model is being established. The simplified DE film and frame deformation are shown in Figure 7. Let  $\theta$  be the joint bending angle, and in the ideal situation, deformation of the DEMES would be as shown in Figure 7.

The output torque can be described as

$$T_{\text{output}} = T_{\text{film}} \cdot f(U_{\text{film}}) - T_{\text{frame}}, \quad (1)$$

where  $T_{\text{film}}$  is the bending torque of force  $F$  on the frame,  $T_{\text{frame}}$  is the restoring torque of the frame, and  $f$  is a function related to the voltage on the film  $U_{\text{film}}$  defined as

$$f(U_{\text{film}}) = \begin{cases} 1 & U_{\text{film}} = 0 \\ (0, 1) & 0 < U_{\text{film}} < U_c \\ 0 & U_c \leq U_{\text{film}}, \end{cases} \quad (2)$$

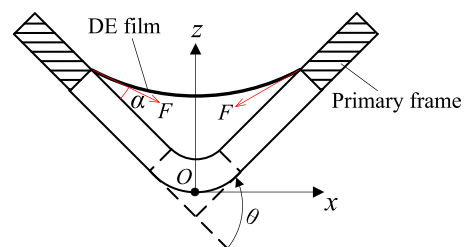


FIG. 7. Cross section of the DEMES in static equilibrium.

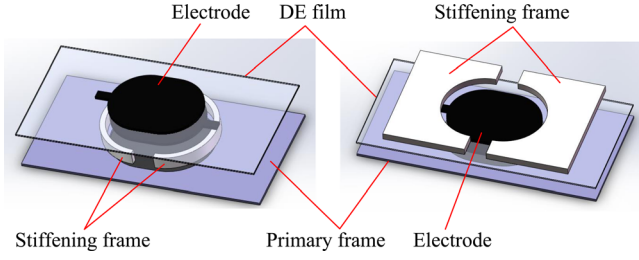


FIG. 8. Comparison between the new and old DEMES. (a) The new structure. (b) The old structure.

where  $U_c$  is a critical voltage that makes the stress in the film disappear. If we ignore any rigidity of the DE film and deformation of the stiffening frame, the relationship between  $T_{\text{frame}}$  and the bending angle  $\theta$  can be obtained as Equation (3), which is based on beam bending analysis.<sup>15</sup> We have

$$T_{\text{frame}} = \frac{E(w - 2r)t^3}{12s} \theta, \quad (3)$$

where  $E$  is the Young's modulus of the frame, and  $w$ ,  $r$ ,  $t$ , and  $s$  have been defined in Figure 6. Therefore, to increase  $T_{\text{output}}$ , we should increase  $T_{\text{film}}$ , resulting in a new structure as shown in Figure 8.

The cross section in  $xOz$  plane and static equilibrium of the DEMES are shown in Figure 9.

Let us choose the bending torque of section  $m-m$  to compare to the torque of films  $T_{\text{film1}}$  and  $T_{\text{film2}}$ , the torque is with regard to the middle point  $M$  within the section  $m-m$ , so it can be calculated by Equations (4) and (5). The section  $m-m$  and point  $M$  is shown in Figure 9.

The bending torque  $T_{\text{film1}}$  and  $T_{\text{film2}}$  in section  $m-m$  can be calculated as follows:

$$T_{\text{film1}} = F_1 t_1 \cos \alpha_1 / 2 + F_1 r \sin \alpha_1, \quad (4)$$

$$T_{\text{film2}} = F_2 (t_2 / 2 + p) \cos \alpha_2 + F_2 r \sin \alpha_2. \quad (5)$$

Actually, in the general application,  $r$  is much larger than  $p$ , so the influence of  $p$  to morphology of the film is negligible with rough calculation. Thus, we can consider  $F_1 \approx F_2$ ,  $\alpha_1 \approx \alpha_2$  and denote a specific value  $\lambda$  by which to compare  $T_{\text{film2}}$  and  $T_{\text{film1}}$  in Equation (6). If we let  $\alpha_1 = \alpha_2 = \alpha$  while  $t_1 = t_2 = t$ , then  $\lambda$  can be calculated by the approximation

$$\lambda = \frac{T_{\text{film2}}}{T_{\text{film1}}} = \frac{F_2 (t_2 / 2 + p) \cos \alpha_2 + F_2 r \sin \alpha_2}{F_1 t_1 \cos \alpha_1 / 2 + F_1 r \sin \alpha_1} \approx 1 + \frac{p}{t/2 + r \tan \alpha}. \quad (6)$$

According to Equation (6),  $T_{\text{film2}} > T_{\text{film1}}$ , so the torque of the film with the new structure is larger than that of the old, and  $\lambda$

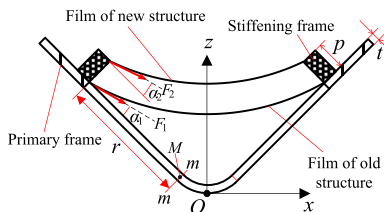


FIG. 9. Cross section in  $xOz$  plane of the new and old structures.

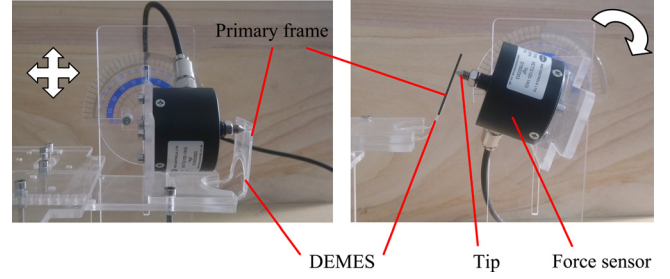


FIG. 10. The system to measure torque of the DEMES. (a) Measurement of  $T_{\text{output}}$ . (b) Measurement of  $T_{\text{frame}}$ .

will increase with  $p$  because  $p$  does not influence  $\alpha$ , while  $r$  is much larger than  $p$ . On the other hand, it can be seen from Figure 2 that the larger the bending angle  $\theta$ , the larger that  $F_z$  and  $a$  will be, and the smaller  $\lambda$  becomes in Equation (6).

To validate the above analysis and the improvement on the output torque, the torques of a film with a new and an old structure should be measured. A 400% biaxial pre-strain is chosen with VHB 4910; thus the film can maintain at least 254% pre-strain at a 90° initial angle of the DEMES. The 254% pre-strain is calculated by Equation (7) with  $\varepsilon_0 = 4$  from geometric analysis

$$\varepsilon_m = \frac{\sqrt{2}(1 + \varepsilon_0)l_0 - 2l_0}{2l_0}, \quad (7)$$

where  $\varepsilon_m$  is the maintained pre-strain,  $\varepsilon_0$  is the initial pre-strain, and  $l_0 = 2r + s$ ,  $r$  and  $s$  are defined in Figure 6.  $\varepsilon_m = 254\%$ , while  $\varepsilon_0 = 400\%$ . The primary frame is made of laser-cut PET with a Young's modulus of 6.08 GPa, and the stiffening frame of the new structure is made of laser-cut polymethyl methacrylate (PMMA) with a Young's modulus of 2.9 GPa. Specially, 400% biaxially pre-strained VHB 4910 is attached to the PMMA before laser-cutting. Thus, the PMMA can be glued to the primary frame. More fabrication details can be seen in Ref. 16.

The measurements of output torque were conducted on the system shown in Figure 10. Specifically, the miniature load cells (MCTG100-1 Kg) have three degrees of freedom to ensure the tip remains perpendicular to the primary frame and contacts at same point of the DEMES.

We tested three kinds of structures with an initial angle of around 90° as shown in Table I.

To validate Equation (6), using the measurement results of three structures shown in Table I, the flow diagram is as follow:

Step 1: Calculate the torques  $T_{\text{film}}$  by Equations (1) and (2) by measurement of  $T_{\text{frame}}$  and  $T_{\text{output}}$  with  $U_{\text{film}} = 0$ .

Step 2: Calculate  $\alpha$  by Equation (6) using the measurement results  $T_{\text{film1}}$  of Old-thick and  $T_{\text{film2}}$  of New-thick.

TABLE I. Parameters of the three structures (unit: mm).

Number of the structures	Name of the structures	$w$	$p$	$q$	$t$	$l$	$s$	$r$
1	Old-thick	40	0.25	30	0.188	88	8	15
2	New-thick	49	1	3	0.188	88	8	15
3	Old-thin	57	0.25	30	0.125	88	8	15



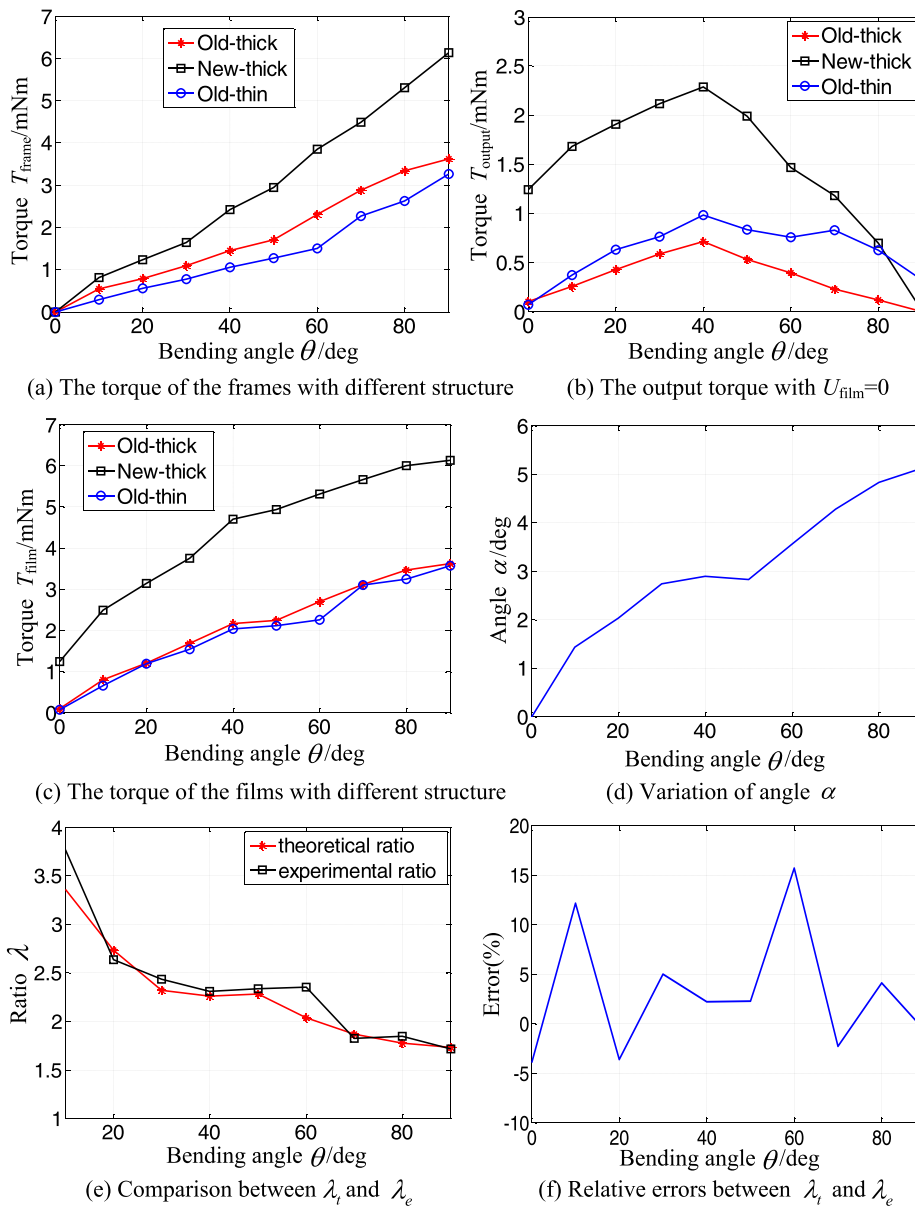


FIG. 11. Experimental results with different structures, single layer of VHB 4910.

Step 3: Calculate the ratio  $\lambda_{t,2-3}$  between New-thick and Old-thin by above  $\alpha$  and Equation (6).

Step 4: Calculate the ratio  $\lambda_{e,2-3}$  by  $T_{\text{film}}$  of New-thick and Old-thin in step 1.

Step 5: Compare the theoretical ratio  $\lambda_{t,2-3}$  and the experimental ratio  $\lambda_{e,2-3}$ .

The experimental results of above parameters with different structures are shown in Figure 11, respectively.

Based on theoretical analysis,  $\alpha$  will increase with angle  $\theta$  that has been validated by Figure 11(d);  $\lambda$  will decrease with angle  $\theta$  that has been validated by Figure 11(e).  $\lambda > 1$  indicates the increase of output torque of the DEMES with the new structure. The relative error between  $\lambda_t$  and  $\lambda_e$  is large because the DEMES is fabricated by handwork and the repeatability is poor; on the other hand, the approximation in Equation (6) will introduce error too.

In summary, the morphology of a DE film on a DEMES is a saddle surface, and the output torque of the DEMES can be improved by redesigning its structure. The thicker the stiffening frame, the larger the output torque will be. As an

example, the torque of the film with the new structure (parameters are shown in Table I) is larger than 1.7 times that of the old structure. This new DEMES structure can be applied to a rotary joint of a flapping wing or other soft mobile robot, notably because the new DEMES structure will reduce power requirements with same payload capacity.

This work was supported by National Natural Science Foundation of China (Grant No. 51205076) and China Postdoctoral Science Foundation (Grant No. 2013M541359).

<sup>1</sup>R. Pelrine, R. Kornbluh, Q. Pei, and J. Joseph, *Science* **287**, 836 (2000).

<sup>2</sup>A. Wingert, M. D. Lichter, and S. Dubowsky, *IEEE/ASME Trans. Mechatron.* **11**, 448–456 (2006).

<sup>3</sup>M. Karpelson, G. Y. Wei, and R. J. Wood, in *2008 IEEE International Conference on Robotics and Automation (ICRA)* (IEEE, 2008), pp. 779–786.

<sup>4</sup>G. Kofod, W. Wirges, M. Paajanen, and S. Bauer, *Appl. Phys. Lett.* **90**, 081916 (2007).

<sup>5</sup>C. H. Nguyen, G. Alici, and R. Mutlu, in *2014 IEEE/ASME International Conference on Advanced Intelligent Mechatronics (AIM)* (IEEE, 2014), pp. 599–604.

- <sup>6</sup>S. Rosset, O. A. Araromi, J. Shintake, and H. R. Shea, *Smart Mater. Struct.* **23**, 085021 (2014).
- <sup>7</sup>B. O'Brien, T. Gisby, E. Calius, S. Xie, and I. Anderson, *Proc. SPIE* **7287**, 728706 (2009).
- <sup>8</sup>S. Siu, L. Rhode-Barbarigos, S. Wagner, and S. Adriaenssens, *Appl. Phys. Lett.* **103**, 171906 (2013).
- <sup>9</sup>G. Buchberger, B. Hauser, J. Schoeftner, S. Bauer, B. Jakoby, and W. Hilber, *J. Appl. Phys.* **115**, 214105 (2014).
- <sup>10</sup>J. Zhao, J. Niu, D. McCoul, R. Zhi, and Q. Pei, *Appl. Phys. Lett.* **106**, 133504 (2015).
- <sup>11</sup>M. T. Petralia and R. J. Wood, in *IEEE/RSJ International Conference on Intelligent Robots and Systems* (IEEE, 2010), pp. 2357–2363.
- <sup>12</sup>J. Zhao, J. Niu, L. Liu, and J. Yu, *Proc. SPIE* **9056**, 905608 (2014).
- <sup>13</sup>O. A. Araromi, I. Gavrilovich, J. Shintake, S. Rosset, M. Richard, V. Gass, and H. R. Shea, *IEEE/ASME Trans. Mechatron.* **20**, 438–446 (2015).
- <sup>14</sup>G. Kofod, M. Paajanen, and S. Bauer, *Appl. Phys. A* **85**, 141–143 (2006).
- <sup>15</sup>J. M. Gere and B. J. Goodno, *Mechanics of Materials*, 7th ed. (Cengage Learning, Inc., 2009), pp. 356–366.
- <sup>16</sup>W. Lai, A. F. Bastawros, W. Hong, and S. J. Chung, in *IEEE International Conference on Robotics and Automation (ICRA)* (IEEE, 2012), pp. 4968–4973.